Catheterization and Cardiovascular Interventions 67:637–643 (2006)

Real-Time MRI Guided Atrial Septal Puncture and Balloon Septostomy in Swine

Amish N. Raval,[1] MD, Parag V. Karmarkar,[1,2] MSc, Michael A. Guttman,[3] MSc, Cengizhan Ozturk,[1] MD, PhD, Ranil DeSilva,[1] MBBS, PhD, Ronnier J. Aviles,[1] MD, Victor J. Wright,[1] BS, William H. Schenke,[1] BS, Ergin Atalar,[2] PhD, Elliot R. McVeigh,[3] PhD, and Robert J. Lederman,[1]* MD

Cardiac perforation during atrial septal puncture (ASP) might be avoided by improved image guidance. X-ray fluoroscopy (XRF), which guides ASP, visualizes tissue poorly and does not convey depth information. Ultrasound is limited by device shadows and constrained imaging windows. Alternatively, real-time MRI (rtMRI) provides excellent tissue contrast in any orientation and may enable ASP and balloon atrial septostomy (BAS) in swine. Custom MRI catheters incorporated "active" (receiver antenna) and "passive" (iron or gadolinium) elements. Wholly rtMRI-guided transfemoral ASP and BAS were performed in 10 swine in a 1.5T interventional suite. Hemodynamic results were measured with catheters and velocity encoded MRI. Successful ASP was performed in all 10 animals. Necropsy confirmed septostomy confined within the fossa ovalis in all. BAS was successful in 9/10 animals. Antenna failure in a re-used needle led to inadvertent vena cava tear prior to BAS in 1 animal. ASP in the same animal was easily performed using a new needle. rtMRI illustrated clear device-tissue-lumen relationships in multiple orientations, and facilitated simple ASP and BAS. The mean procedure time was 19 ± 10 minutes. Septostomy achieved a mean left to right shunt ratio of 1.3:1 in these healthy animals. Interactive rtMRI permits rapid transcatheter ASP and BAS in swine. Further technical development may enable novel applications.

Key words: atrial septal puncture; congenital heart disease; real-time magnetic resonance imaging; interventional MRI; magnetic resonance

INTRODUCTION

Atrial septal puncture (ASP) [1,2] is an initial step in a variety of procedures requiring transvenous left atrial entry. Despite years of experience, complications such as cardiac perforation still occur and may relate to limitations of X-ray fluoroscopy (XRF) or ultrasound image guidance [3–12]. For example, XRF requires ASP to be performed relatively blindly. XRF uses ionizing radiation, discriminates tissue poorly, and displays projections (shadows) that lack depth information. Ultrasound is constrained by limited acoustic windows, narrow fields of view, and device-related shadow artifacts.

Alternatively, magnetic resonance imaging (MRI) provides tissue imaging with good contrast, in any user-defined plane, without exposure to ionizing radiation or nephrotoxic contrast agents. Technical advances now permit real-time MRI (rtMRI) to guide catheter based procedures [13–33]. We are developing interactive, multi-slice rtMRI to guide precise catheter-based connection of vascular structures across tissue boundaries. To

[1]Cardiovascular Branch, Division of Intramural Research, National Heart Lung and Blood Institute, National Institutes of Health, Bethesda, Maryland
[2]Department of Radiology, The Johns Hopkins University, Baltimore, Maryland
[3]Laboratory of Cardiac Energetics, Division of Intramural Research, National Heart Lung and Blood Institute, National Institutes of Health, Bethesda, Maryland

This article contains Supplementary Material available at http://interscience.wiley.com/jpages/1522-1946/suppmat/

A.N. Raval and P.V. Karmarkar contributed equally to this work.

*Correspondence to: Dr. Robert J. Lederman, Cardiovascular Branch, Division of Intramural Research, National Heart, Lung, and Blood Institute, National Institutes of Health, Building 10, Room 2c713, MSC 1538, Bethesda, MD 20892-1538.
E-mail: lederman@nih.gov

Received 11 October 2005; accepted 17 October 2005

DOI 10.1002/ccd.20579
Published online 13 March 2006 in Wiley InterScience (www.interscience.wiley.com).

test this concept, we demonstrate rtMRI-guided ASP with subsequent balloon atrial septostomy (BAS) in swine.

METHODS

Animal Protocol

Animal protocols were approved by the National Heart, Lung, and Blood Institute Animal Care and Use Committee. Ten healthy juvenile NIH miniswine weighing 19–60kg (mean 38 ± 14kg) were pretreated with aspirin. MRI confirmed no pre-existing patent foramen ovale or atrial septal defect. Intravenous heparin 100U/kg was administered after percutaneous sheath access of femoral veins, and supplemented after atrial septal puncture. Baseline and post procedure pressures and oximetry were measured using a pulmonary artery catheter. Oximetric shunt ratio was calculated using the simplified formula:

$$\frac{\text{Pulmonary flow}}{\text{Systemic flow}} = \frac{Q_P}{Q_S} = \frac{SAO_2\% - MVO_2\%}{SAO_2\% - PAO_2\%}$$

where $SAO_2\%$, $PAO_2\%$, and $MVO_2\%$ represent hemoglobin oxygen saturation in systemic artery, pulmonary artery, and mixed venous blood samples, respectively. $MVO_2\%$ was estimated as [(2 × Superior vena cava O2%) + (Inferior vena cava O2%)] ÷ 3 [34]. Following euthanasia, hearts were explanted for examination.

Interventional MRI Suite

rtMRI guided ASP and BAS were performed in a clinical interventional MRI suite [35] (1.5T, Sonata, Siemens). MRI data were transferred during acquisition via Gigabit Ethernet to an external workstation for rapid reconstruction [36,37]. Hemodynamics, scan control, and volume-rendered images were displayed inside the scanner room using shielded LCD projectors. The MR-compatible monitoring system displayed oximetry, two-channel invasive blood pressure, and surface electrocardiogram. (Magnitude CV, In-Vivo Research) Standard 6 channel phased array torso and spine surface coils were used. The operators and staff communicated via directional optical microphones (PhoneOr) and RF-filtered headsets fitted with active sound suppression (Magnacoustics).

Image data derived from catheter antennae were displayed in color, whereas image data derived from surface MRI coils were displayed in grayscale. When required, catheter images could be imaged even when outside of selected scanning slabs by using projection-mode MRI (disabling slice-select). The frame rate could be doubled interactively using echo-sharing, wherein MRI image data were interleaved over temporally adjacent frames. Saturation pre-pulses were toggled on/off during real-time imaging to suppress background tissue when gadolinium contrast enhancement was desired. ECG gating was toggled on/off to suspend cardiac motion, and temporal image filtering (averaging) was applied without scan interruption to improve signal-to-noise ratio (SNR). Multiple oblique slices were acquired in rapid succession, repositioned interactively, or individually omitted and reapplied as desired.

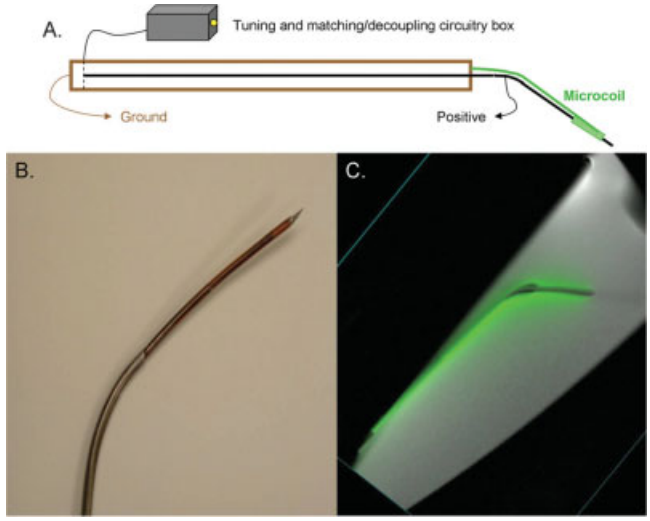

Fig. 1. "Active" ASP needle. A: Schematic of the custom modified loopless antenna ASP needle. To enhance tip visibility, a microcoil is affixed to the distal tip (positive) and connected to the outer shaft (ground). Appropriate tuning, matching, and decoupling circuitry connect the needle to an MRI receiver channel. B: Photograph of 6F ASP needle. C: Image of the active ASP needle colored green in a water phantom.

Magnetic Resonance Imaging

Catheter manipulations were guided by imaging in real-time with steady state free precession (SSFP) pulse sequences. Typical parameters were repetition time (TR) 2.8 ms, echo time (TE) 1.4 ms, flip angle 45°, bandwidth 800 Hz/pixel, FOV 32 × 24 cm, matrix 192 × 108, generating 1.7 × 2.2 × 6 mm voxels. Using echo-sharing, an imaging rate of 8 frames/s was achieved with an acquisition-to-display latency of approximately 250 ms.

Baseline and post procedure 2-dimensional through-plane phase contrast MRI (PC-MRI) was performed on axial slices through the ascending aorta (AA) and main pulmonary artery (PA). Typical parameters were TR/TE 33/3 ms, flip angle 30°, FOV 28 cm, velocity encoding 350 cm/sec, bandwidth 1528 Hz/pixel, matrix 256 × 256, and slice thickness 5mm. Manual segmentation on each phase was performed for flow quantification (Argus VA50C, Siemens). For each axial PA or

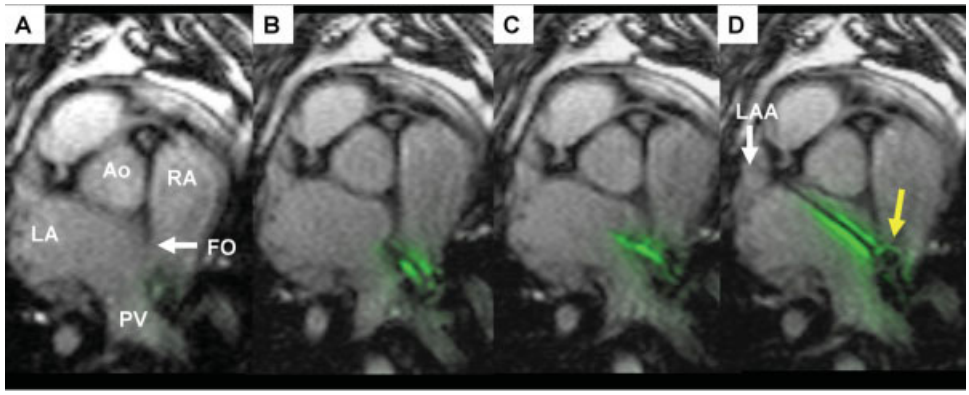

Fig. 2. Atrial septal puncture procedure sequence. A: Baseline transverse slice imaged in real time. Ao = aorta, RA = right atrium, LA = left atrium, FO = fossa ovalis (white arrow), PV = pulmonary vein. B: The modified "active" ASP needle (green) can be seen tenting the interatrial septum at the level of the fossa ovalis. C: The needle tip has entered into the LA. D: A floppy-tipped 0.018-inch wire is advanced through the needle into the LA and subsequently left atrial appendage (LAA). It has coupled with the needle signal and, therefore, appears green. The dilator sheath tip susceptibility marker can be seen abutting the RA side of the septum (yellow arrow).

AA slice, two measurements, obtained 1–3 minutes apart, were averaged.

Invasive Devices

Custom MRI compatible catheter devices were made visible by incorporating ''active'' signal receiver coils, or ''passive'' elements causing signal voids (i.e., steel) or signal enhancement (i.e., gadolinium).

Active Devices. Custom 1.7 mm diameter (6F) ASP needles were designed as loopless antennae [38] containing telescoping nitinol hypotubes separated by polyimide insulation (Fig. 1). Tuning, matching, and decoupling circuitry, attached at the proximal hub, were connected to a separate MR scanner receiver channel. An 0.018-inch lumen permitted wire or contrast delivery, but not pressure transduction. Active, dipole flexible-tipped 0.032-inch guide wires were custom manufactured to deliver septostomy balloons. Loopless antenna designs permit visualization of devices along their entire length [38], without significant heating [39–41].

Heating of the ASP needle was tested *in vitro* in a 4% polyacrylamide gel phantom (conductivity 0.7 S/m). Scanning conditions were designed to exaggerate heating, including positioning 20 cm away from the bore center, and continuous gradient echo MRI with a high flip angle ($\alpha = 90^\circ$, TR/TE = 3.4/1.6 ms), generating an input specific absorption rate of 3.7 W/kg. Temperature was measured at steady state using five fiberoptic thermistor probes (Umi-8, Fiso Technologies) placed along the length of the device, including the tip.

Passive Devices. 6F dilator (for ASP needle) and 10F introducer sheaths (for largest BAS balloon) were trimmed and angled (Fast Cath, St. Jude; BriteTip, Cordis) using a heat gun. Single 0.014-inch diameter $\times$ 1 mm length 316L stainless steel markers were bonded to the distal tip of each sheath to create discrete MRI signal voids. Progressively larger angioplasty balloons (Agiltrac 8-, 10-, and 14 $\times$ 20mm, Guidant) were inflated at nominal pressures with 5mM gadopentate dimeglumine (Gd-DTPA, Magnevist, Berlex). Septostomy dimensions were measured under MRI and XRF using atrial sizing balloons (Amplatzer, AGA Medical).

Statistics

Continuous parameters were reported as mean $\pm$ standard deviation and were compared using Student's t-test. A value of $P < 0.05$ was considered significant.

RESULTS

In a static phantom, the tip of the active ASP needle increased 6.3°C during 10 minutes of continuous MRI. Under the same conditions, a redesigned needle with additional polyester insulation heated 2.5°C at the tip, without significantly altering the crossing profile.

Following femoral venous insertion of the introducer sheath, the active needle and transseptal sheath were advanced in tandem into the right atrium under rtMRI guidance. The needle was steered in real time to appose the fossa ovalis, guided by imaging in multiple slice planes. Accurate positioning was confirmed with interactive application of ECG-gated rtMRI. ASP was then performed by simple needle advancement (Fig. 2). Once the needle entered the left atrium under rtMRI, confirmatory MR angiography was performed by injecting 3–5mL dilute Gd-DTPA (30mM) under real-time SSFP with a non-selective saturation prepulse (Fig. 3). Next, a guidewire was advanced into the left atrium and used to intro-

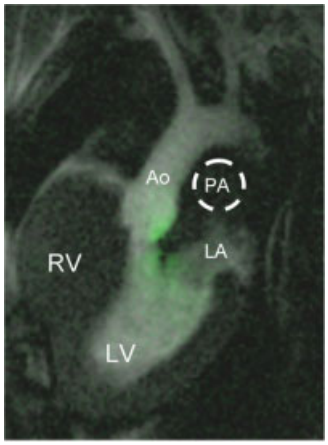

Fig. 3. Selective real-time MR angiogram confirming ASP needle entry into the left atrium. After visual confirmation of ASP needle entry in the left atrium, 3–5mL of 30mM dilute Gd-DTPA is injected through the ASP needle wire port. A saturation pre-pulse is applied to suppress the background as contrast sequentially enhances the lumen of the left atrium (LA), left ventricle (LV), and out the aorta (Ao). Note there is no contrast enhancement of the right ventricle (RV) or outlined pulmonary artery (PA), indicating successful ASP.

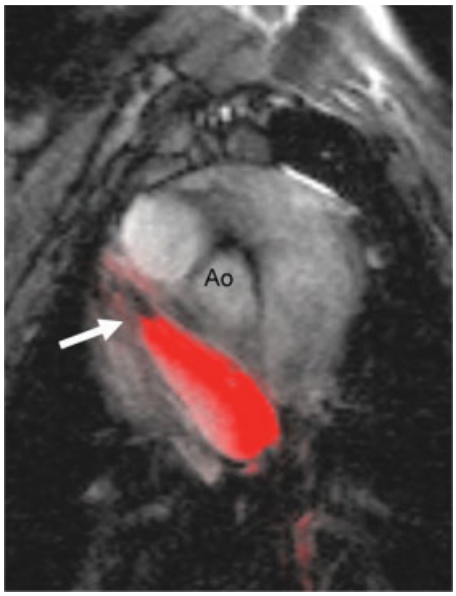

Fig. 4. Balloon atrial septostomy. A 14 mm × 40mm peripheral angioplasty balloon (red) inflated with dilute Gd-DTPA across the interatrial septum. A platinum marker indicates the distal aspect of the balloon (white arrow). The proximal marker is out of plane. Ao = aorta.

duce the dilator sheath and thereby record left atrial pressure. BAS was then performed using three incrementally larger (8–14mm) balloons over the active flexible-tipped guidewire (Fig. 4). In three pigs, post-septostomy defect size was 1.6 ± 0.6 cm using an atrial sizing balloon under both rtMRI and XRF (data not shown).

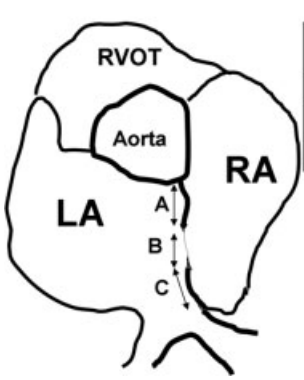

Atrial Septum Dimensions

Site of measurement	Mean length (mm) ± SD
A	11.7 ± 1.9
B	8.0 ± 2.0
C	11.7 ± 3.1

Fig. 5. Atrial septal measurements. Atrial septal dimensions (A–C) obtained from SSFP short axis view. A: Posterior aortic wall to anterior edge of fossa ovalis. B: Fossa ovalis. C: Posterior edge of fossa ovalis to posterior atrial wall. LA = left atrium, RA = right atrium, RVOT = right ventricular outflow track, SD = standard deviation.

ASP was successfully accomplished in all 10 animals. rtMRI permitted anatomic measurements (Fig. 5) and easy navigation with attention to important structures, such as the fossa ovalis, aorta, and posterior atrial wall (see video supplement at http://interscience.wiley.com/jpages/1522-1946/suppmat/). In 1 animal, the tuning/matching/decoupling circuit connection to a repeatedly used active needle was damaged and rendered the device intermittently invisible. This led to inadvertent perforation of the inferior vena cava, causing hemothorax immediately evident by rtMRI. ASP was subsequently successful in this animal using a new needle system, but there was hemodynamic collapse before septostomy could be attempted. BAS was performed without complication in all remaining animals. No animal had a pericardial effusion after at least one hour of observation under MRI.

ASP required 19 ± 10 min (range 6–33, n = 10) from the first rtMRI scan. The average ASP time did not decline from the first five to the last five animals. BAS required 51 ± 16 min (range 31–81, n = 9) from the first rtMRI. BAS increased mean pulmonary artery (PA) pressure (24 ± 6mmHg vs. baseline 14 ± 5 mmHg, $P < 0.01$) but not pulmonary artery wedge (PAW: 12 ± 4 vs. baseline 11 ± 4mmHg, $P = 0.4$) or right atrial (RA) pressure (8 ± 2 vs. baseline 8 ± 3 mmHg, $P = 0.9$). The directly measured left atrial pressure after BAS was 12 ± 3mmHg. BAS increased the mean left to right shunt from 1.0 ± 0.1 at baseline to 1.3 ± 0.2 by oximetry and by PCMRI in these otherwise healthy swine.

Necropsy revealed a large inter-atrial communication confined within the fossa ovalis following BAS in all cases (Fig. 6). In addition, there was no visible evidence of acute thermal injury, thrombus, valve injury, or pericardial effusion in any animal.

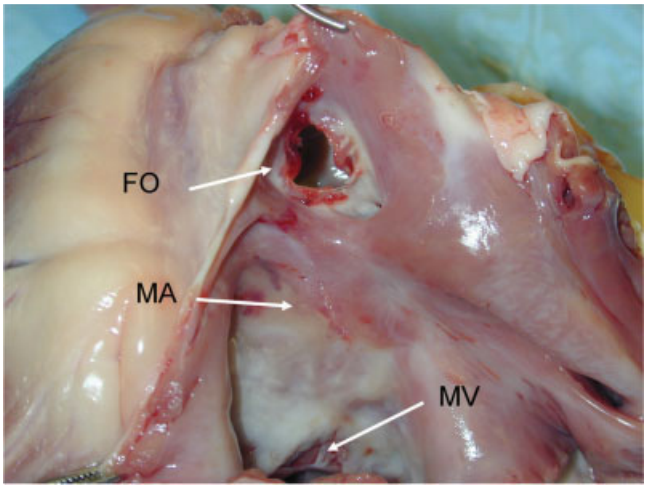

Fig. 6. Necropsy photograph after BAS view from the left atrium. The septostomy is centered within the fossa ovalis (FO). There is no gross evidence of thermal injury or valve disruption. MA = mitral annulus, MV = mitral valve.

DISCUSSION

This report demonstrates rapid and ''comfortable'' conduct of atrial septal puncture and balloon septostomy entirely using rtMRI and custom catheter devices in swine.

XRF guided ASP was first described by Ross [2,42] and Cope [1], refined by Brockenbrough [43] and Mullins [3], and further improved with adjunctive intracardiac [44] and transesophageal echocardiography [45]. Examples of procedures that require transeptal access include percutaneous mitral valvuloplasty [46], radiofrequency ablation for arrhythmia [47,48], and balloon atrial septostomy in congenital heart diseases [49] or severe pulmonary artery hypertension [50]. Emerging indications include left atrial appendage occlusion for chronic atrial fibrillation [51], and percutaneous mitral [52] or aortic valve repair [53]. Despite decades of experience, even highly skilled operators cause cardiac perforation during transeptal puncture as often as 0.9–5.4% [3–5,10,11,54–59]. This potentially lethal complication is more likely in patients with very small or large atria, dilated aortic root, thoracic spine deformities, and prior atrial septal defect closure [6]. Transesophageal echo is uncomfortable, requires heavy sedation and pharyngeal and esophageal instrumentation, prolongs procedure time, and inhibits patient communication. Intracardiac echo also suffers from device related shadow artifacts, requires an additional large access sheath, and can interfere mechanically with other interventional devices. With appropriate clinical grade devices, rtMRI might reduce risk and offer robust procedural guidance by better visualizing the interaction between tissue and devices.

MRI guided endovascular procedures have been successfully performed for a variety of preclinical [13–30] and clinical [31–33] indications. In particular, rtMRI device navigation for catheterization [23] and atrial septal defect closure [20,22,29], have been demonstrated using active and passive devices. These investigators performed ASP under XRF guidance [22,23,29] or employed animals having patent foramen ovale [20]. Arepally et al. [14] demonstrated ASP using a similar active needle. They did not, however, test heating characteristics of the device and did not conduct an interventional procedure or hemodynamic assessment. Moreover, they did not use a clinically suitable rtMRI environment combining colorized device display and interactive multi-slice imaging [30]. Kee et al. created transjugular intrahepatic portosystemic shunts (TIPS) using combined XRF and low-field rtMRI in swine [13] and humans [60]. Our contribution demonstrates a complex two stage intervention, real-time multi-planar image display, clinically relevant device visualization, and combined anatomic and hemodynamic endpoint assessment, entirely using MRI.

ASP and TIPS are examples of procedures in which devices traverse tissue boundaries, and are well suited for rtMRI guidance because of simultaneous device and soft tissue imaging. Combined with appropriate anastomotic devices, this technology might be extended to traverse greater distances for catheter-based connection of disparate vascular chambers, as in peripheral artery bypass or palliative pediatric cardiovascular shunts. Simple adaptations of these catheter devices might facilitate safer image-guided recanalization of peripheral artery occlusions.

In this experience, the rtMRI images portraying both devices and soft tissue were sufficiently information-rich to distinguish important structures simply and comfortably for the ASP operator, even though both spatial and temporal resolution were reduced compared with XRF (192×128 pixels and 8 frames/s compared with 512–1024 square and 15–30 frames/s). The enhanced tissue visualization averted iatrogenic aortic penetration, a potentially catastrophic complication that might not have been prevented using XRF or ultrasound. On a related note, interactive rtMRI may enhance procedural safety by identifying unexpected complications early. In one pig, hemorrhage was immediately evident under rtMRI; pericardial effusion would similarly be readily evident. This information might expedite emergency treatment in a clinical setting.

One limitation of this work is that catheter devices were homemade. Imaging failure in one such device led to catastrophic complication, underscoring the importance of safe, durable, conspicuous clinical-grade instruments. These experiments were performed in nor-

mal swine and, therefore, do not test the potential of MRI-guided therapy in complex clinical conditions. As predicted, the observed acute shunt was low using positive pressure ventilation with positive end-expiratory pressure. Nevertheless, necropsy consistently confirmed accurate anatomic positioning of ASP in all animals within the center of the fossa ovalis.

In conclusion, rtMRI permits rapid and robust transcatheter ASP and BAS by virtue of superior visualization of complex anatomy in any orientation. Additional advantages include online hemodynamic assessment and freedom from exposure to ionizing radiation or nephrotoxic contrast agents. Further technical development may enable more novel applications.

PRACTICAL APPLICATIONS

Conducting atrial septal puncture and balloon septostomy under real-time MRI guidance may enhance procedural safety, speed, and operator confidence. Human translation of these findings will require development of clinical-grade catheter devices.

REFERENCES

1. Cope C. Technique for transseptal catheterization of the left atrium; preliminary report. J Thorac Surg 1959;37:482–486.
2. Ross J Jr, Braunwald E, Morrow AG. Transseptal left atrial puncture; new technique for the measurement of left atrial pressure in man. Am J Cardiol 1959;3:653–655.
3. Mullins CE. Transseptal left heart catheterization: experience with a new technique in 520 pediatric and adult patients. Pediatr Cardiol 1983;4:239–245.
4. Braunwald E. Cooperative study on cardiac catheterization. Transseptal left heart catheterization. Circulation 1968;37:III74–III79.
5. Friedrich SP, Berman AD, Baim DS, Diver DJ. Myocardial perforation in the cardiac catheterization laboratory: incidence, presentation, diagnosis, and management. Cathet Cardiovasc Diagn 1994;32:99–107.
6. Bloomfield DA, Sinclair-Smith BC. The limbic ledge. A landmark for transseptal left heart catheterization. Circulation 1965;31:103–107.
7. Venables AW. Balloon atrial septostomy in complete transposition of great arteries in infancy. Br Heart J 1970;32:61–65.
8. Allen HD, Beekman RH 3rd, Garson A Jr, Hijazi ZM, Mullins C, O'Laughlin MP, Taubert KA. Pediatric therapeutic cardiac catheterization: a statement for healthcare professionals from the Council on Cardiovascular Disease in the Young, American Heart Association. Circulation 1998;97:609–625.
9. El-Said HG, Ing FF, Grifka RG, Nihill MR, Morris C, Getty-Houswright D, Mullins CE. 18-year experience with transseptal procedures through baffles, conduits, and other intra-atrial patches. Catheter Cardiovasc Interv 2000;50:434–439; discussion 440.
10. Park SW, Gwon HC, Jeong JO, Byun J, Kang HS, You JR, Cho SS, Lee MJ, Lee Y, Kim S, et al. Intracardiac echocardiographic guidance and monitoring during percutaneous endomyocardial gene injection in porcine heart. Hum Gene Ther 2001;12:893–903.
11. Croft CH, Lipscomb K. Modified technique of transseptal left heart catheterization. J Am Coll Cardiol 1985;5:904–910.
12. Schroeder VA, Shim D, Spicer RL, Pearl JM, Manning PJ, Beekman RH 3rd. Surgical emergencies during pediatric interventional catheterization. J Pediatr 2002;140:570–575.
13. Kee ST, Rhee JS, Butts K, Daniel B, Pauly J, Kerr A, O'Sullivan GJ, Sze DY, Razavi MK, Semba CP, et al. 1999 Gary J. Becker Young Investigator Award. MR-guided transjugular portosystemic shunt placement in a swine model. J Vasc Interv Radiol 1999;10:529–535.
14. Arepally A, Karmarkar PV, Weiss C, Rodriguez ER, Lederman RJ, Atalar E. Magnetic resonance image-guided trans-septal puncture in a swine heart. J Magn Reson Imaging 2005;21:463–467.
15. Strother CM, Unal O, Frayne R, Turk A, Omary R, Korosec FR, Mistretta CA. Endovascular treatment of experimental canine aneurysms: feasibility with MR imaging guidance. Radiology 2000;215:516–519.
16. Bartels LW, Bos C, van Der Weide R, Smits HF, Bakker CJ, Viergever MA. Placement of an inferior vena cava filter in a pig guided by high-resolution MR fluoroscopy at 1.5 T. J Magn Reson Imaging 2000;12:599–605.
17. Omary RA, Frayne R, Unal O, Warner T, Korosec FR, Mistretta CA, Strother CM, Grist TM. MR-guided angioplasty of renal artery stenosis in a pig model: a feasibility study. J Vasc Interv Radiol 2000;11:373–381.
18. Bucker A, Neuerburg JM, Adam GB, Glowinski A, Schaeffter T, Rasche V, van Vaals JJ, Gunther RW. Real-time MR guidance for inferior vena cava filter placement in an animal model. J Vasc Interv Radiol 2001;12:753–756.
19. Buecker A, Adam GB, Neuerburg JM, Kinzel S, Glowinski A, Schaeffter T, Rasche V, van Vaals JJ, Guenther RW. Simultaneous real-time visualization of the catheter tip and vascular anatomy for MR-guided PTA of iliac arteries in an animal model. J Magn Reson Imaging 2002;16:201–208.
20. Buecker A, Spuentrup E, Grabitz R, Freudenthal F, Muehler EG, Schaeffter T, van Vaals JJ, Gunther RW. Magnetic resonance-guided placement of atrial septal closure device in animal model of patent foramen ovale. Circulation 2002;106:511–515.
21. Spuentrup E, Ruebben A, Schaeffter T, Manning WJ, Gunther RW, Buecker A. Magnetic resonance-guided coronary artery stent placement in a swine model. Circulation 2002;105:874–879.
22. Rickers C, Jerosch-Herold M, Hu X, Murthy N, Wang X, Kong H, Seethamraju RT, Weil J, Wilke NM. Magnetic resonance image-guided transcatheter closure of atrial septal defects. Circulation 2003;107:132–138.
23. Schalla S, Saeed M, Higgins CB, Martin A, Weber O, Moore P. Magnetic resonance-guided cardiac catheterization in a swine model of atrial septal defect. Circulation 2003;108:1865–1870.
24. Serfaty JM, Yang X, Foo TK, Kumar A, Derbyshire A, Atalar E. MRI-guided coronary catheterization and PTCA: a feasibility study on a dog model. Magn Reson Med 2003;49:258–263.
25. Dick AJ, Guttman MA, Raman VK, Peters DC, Pessanha BS, Hill JM, Smith S, Scott G, McVeigh ER, Lederman RJ. Magnetic resonance fluoroscopy allows targeted delivery of mesenchymal stem cells to infarct borders in swine. Circulation 2003;108:2899–2904.
26. Kuehne T, Yilmaz S, Meinus C, Moore P, Saeed M, Weber O, Higgins CB, Blank T, Elsaesser E, Schnackenburg B, et al. Magnetic resonance imaging-guided transcatheter implantation of a prosthetic valve in aortic valve position: feasibility study in swine. J Am Coll Cardiol 2004;44:2247–2249.
27. Raman VK, Karmarkar PV, Guttman MA, Dick AJ, Peters DC, Ozturk C, Pessanha BS, Thompson RB, Raval AN, DeSilva R, et al. Real-time magnetic resonance-guided endovascular repair of experimental abdominal aortic aneurysm in swine. J Am Coll Cardiol 2005;45:2069–2077.
28. Feng L, Dumoulin CL, Dashnaw S, Darrow RD, Delapaz RL, Bishop PL, Pile-Spellman J. Feasibility of stent placement in carotid arteries with real-time MR imaging guidance in pigs. Radiology 2005;234:558–562.

29. Schalla S, Saeed M, Higgins CB, Weber O, Martin A, Moore P. Balloon sizing and transcatheter closure of acute atrial septal defects guided by magnetic resonance fluoroscopy: assessment and validation in a large animal model. J Magn Reson Imaging 2005;21:204–211.
30. Raval AN, Telep JD, Guttman MA, Ozturk C, Jones M, Thompson RB, Wright VJ, Schenke WH, DeSilva R, Aviles RJ, et al. Real-time magnetic resonance imaging-guided stenting of aortic coarctation with commercially available catheter devices in swine. Circulation 2005;112:699–706.
31. Manke C, Nitz WR, Djavidani B, Strotzer M, Lenhart M, Volk M, Feuerbach S, Link J. MR imaging-guided stent placement in iliac arterial stenoses: a feasibility study. Radiology 2001;219:527–534.
32. Razavi R, Hill DL, Keevil SF, Miquel ME, Muthurangu V, Hegde S, Rhode K, Barnett M, van Vaals J, Hawkes DJ, et al. Cardiac catheterisation guided by MRI in children and adults with congenital heart disease. Lancet 2003;362:1877–1882.
33. Paetzel C, Zorger N, Bachthaler M, Hamer OW, Stehr A, Feuerbach S, Lenhart M, Volk M, Herold T, Kasprzak P, et al. Magnetic resonance-guided percutaneous angioplasty of femoral and popliteal artery stenoses using real-time imaging and intra-arterial contrast-enhanced magnetic resonance angiography. Invest Radiol 2005;40:257–262.
34. Flamm MD, Cohn KE, Hancock EW. Measurement of systemic cardiac output at rest and exercise in patients with atrial septal defect. Am J Cardiol 1969;23:25–265.
35. Dick AJ, Raman VK, Raval AN, Guttman MA, Thompson RB, Ozturk C, Peters DC, Stine AM, Wright VJ, Schenke WH, et al. Invasive human magnetic resonance imaging during angioplasty: feasibility in a combined XMR suite. Catheter Cardiovasc Interv 2005;64:265–274.
36. Guttman MA, McVeigh ER. Techniques for fast stereoscopic MRI. Magn Reson Med 2001;46:317–323.
37. Guttman MA, Lederman RJ, Sorger JM, McVeigh ER. Real-time volume rendered MRI for interventional guidance. J Cardiovasc Magn Reson 2002;4:431–442.
38. Ocali O, Atalar E. Intravascular magnetic resonance imaging using a loopless catheter antenna. Magn Reson Med 1997;37:112–118.
39. Yang X, Yeung CJ, Ji H, Serfaty JM, Atalar E. Thermal effect of intravascular MR imaging using an MR imaging-guidewire: an in vivo laboratory and histopathological evaluation. Med Sci Monit 2002;8:MT113–MT117.
40. Susil RC, Yeung CJ, Atalar E. Intravascular extended sensitivity (IVES) MRI antennas. Magn Reson Med 2003;50:383–390.
41. Yeung CJ, Susil RC, Atalar E. RF safety of wires in interventional MRI: using a safety index. Magn Reson Med 2002;47:187–193.
42. Ross J Jr. Transeptal left heart catheterization: a new method of left atrial puncture. Ann Surg 1959;149:395–401.
43. Brockenbrough E, Braunwald E, Ross J. Transseptal left heart catheterization. Circulation 1962;25:15–21.
44. Mitchel JF, Gillam LD, Sanzobrino BW, Hirst JA, McKay RG. Intracardiac ultrasound imaging during transseptal catheterization. Chest 1995;108:104–108.
45. Tucker KJ, Curtis AB, Murphy J, Conti JB, Kazakis DJ, Geiser EA, Conti CR. Transesophageal echocardiographic guidance of transseptal left heart catheterization during radiofrequency ablation of left-sided accessory pathways in humans. Pacing Clin Electrophysiol 1996;19:272–281.
46. Lock JE, Khalilullah M, Shrivastava S, Bahl V, Keane JF. Percutaneous catheter commissurotomy in rheumatic mitral stenosis. N Engl J Med 1985;313:1515–1518.
47. Hsu LF, Jais P, Sanders P, Garrigue S, Hocini M, Sacher F, Takahashi Y, Rotter M, Pasquie JL, Scavee C, et al. Catheter ablation for atrial fibrillation in congestive heart failure. N Engl J Med 2004;351:2373–2383.
48. De Ponti R, Zardini M, Storti C, Longobardi M, Salerno-Uriarte JA. Trans-septal catheterization for radiofrequency catheter ablation of cardiac arrhythmias. Results and safety of a simplified method. Eur Heart J 1998;19:943–950.
49. Gibbs JL. Congenital heart disease: interventional catheterisation II: opening up venous return, the atrial septum, the arterial duct, aortopulmonary shunts, and aortopulmonary collaterals. Heart 2000; 83:237–240.
50. Klepetko W, Mayer E, Sandoval J, Trulock EP, Vachiery J-L, Dartevelle P, Pepke-Zaba J, Jamieson SW, Lang I, Corris P. Interventional and surgical modalities of treatment for pulmonary arterial hypertension. Journal of the American College of Cardiology 2004;43:S73–S80.
51. Sievert H, Lesh MD, Trepels T, Omran H, Bartorelli A, Della Bella P, Nakai T, Reisman M, DiMario C, Block P, et al. Percutaneous left atrial appendage transcatheter occlusion to prevent stroke in high-risk patients with atrial fibrillation: early clinical experience. Circulation 2002;105:1887–1889.
52. Block PC. Percutaneous mitral valve repair for mitral regurgitation. J Interv Cardiol 2003;16:93–96.
53. Cribier A, Eltchaninoff H, Bash A, Borenstein N, Tron C, Bauer F, Derumeaux G, Anselme F, Laborde F, Leon MB. Percutaneous transcatheter implantation of an aortic valve prosthesis for calcific aortic stenosis: first human case description. Circulation 2002;106:3006–3008.
54. B-Lundqvist C, Olsson SB, Varnauskas E. Transseptal left heart catheterization: a review of 278 studies. Clin Cardiol 1986;9:21–26.
55. Roelke M, Smith AJ, Palacios IF. The technique and safety of transseptal left heart catheterization: the Massachusetts General Hospital experience with 1,279 procedures. Cathet Cardiovasc Diagn 1994;32:332–339.
56. O'Keefe JH Jr, Vlietstra RE, Hanley PC, Seward JB. Revival of the transseptal approach for catheterization of the left atrium and ventricle. Mayo Clin Proc 1985;60:790–795.
57. Schoonmaker FW, Vijay NK, Jantz RD. Left atrial and ventricular transseptal catheterization review: losing skills? Cathet Cardiovasc Diagn 1987;13:233–238.
58. Linker NJ, Fitzpatrick AP. The transseptal approach for ablation of cardiac arrhythmias: experience of 104 procedures. Heart 1998; 79:379–382.
59. Ali Khan MA, Mullins CE, Bash SE, al Yousef S, Nihill MR, Sawyer W. Transseptal left heart catheterisation in infants, children, and young adults. Cathet Cardiovasc Diagn 1989;17:198–201.
60. Kee ST, Ganguly A, Daniel BL, Wen ZBS, Butts K, Shimikawa A, Pelc NJ, Fahrig R, Dake M. MR-guided transjugular intrahepatic portosystemic shunt creation with use of a hybrid radiography/MR system. J Vasc Interv Radiol 2005;16:227–234.

APPENDIX

Abbreviations

AA, Ascending aorta; ASP, Atrial septal puncture; BAS, Balloon atrial septostomy; FOV, Field of view; LCD, Liquid crystal display; Gd-DTPA, Gadopentate dimeglumine; MRI, Magnetic resonance imaging; MVO_2, Mixed venous oxygen saturation; NIH, National Institutes of Health; PA, Pulmonary artery; PAO_2, Pulmonary artery oxygen saturation; PC-MRI, Phase-contrast MRI; rtMRI, Real-time magnetic resonance imaging; SAO_2, Systemic arterial oxygen saturation; SSFP, Steady state free precession MRI; TE, Echo time; TIPS, Transjugular intrahepatic portosystemic shunts; TR, Repetition time; XRF, X-ray fluoroscopy.